The one-dimensional complex Ginzburg–Landau equation in the low dissipation limit

D Goldman and L Sirovich

Center for Fluid Mechanics, Brown University, Providence, RI 02912, USA

Abstract. *Turbulent solutions of the one-dimensional complex Ginzburg–Landau equation when the dissipation is very small are considered. It is found that probability distributions are strictly Gaussian, implying hard turbulence does not occur. Also, no inertial range is observed in the wavenumber spectrum. As expected a linear relation between the attractor dimension and the domain length exists, but the results suggest that the dimension of the inertial manifold is smaller than has been predicted. Finally, universal behaviour in both the wavenumber and Lyapunov exponent spectra is demonstrated.*

1. Introduction

The study of chaos in spatially extended model systems is an important step towards a more complete understanding of complex physical problems such as three-dimensional Navier–Stokes turbulence. One model system which is of particular interest is the complex Ginzburg–Landau (CGL) equation. This partial differential equation arises in the course of analysing many physical problems [2–8], including Rayleigh–Bénard convection [9], and contains the important effects of diffusion, nonlinear dispersion and amplitude-dependent frequency. In addition, solutions of the CGL equation are known to exhibit spatiotemporal chaos for certain parameter ranges, even in one spatial dimension [10, 11]. For these reasons, the CGL equation is felt to be an important testing ground for the mathematical techniques and physical intuition involved in studying turbulent phenomena.

The CGL equation typically describes the nonlinear modulation of a linearly unstable wave close to criticality. It has the basic form

$$\frac{\partial A}{\partial t} = \alpha \nabla^2 A + \gamma A + \beta |A|^2 A \tag{1}$$

where A is a complex amplitude and the parameters α, β and γ, which can be determined for a given physical system, are in general complex. An in-depth survey of the CGL equation appears in [12]. Here we consider the one-dimensional CGL equation written in the normalized form [13, 14]

$$\frac{\partial A}{\partial t} = q^2(c_0 + \mathrm{i})\frac{\partial^2 A}{\partial x^2} + \rho A + (-\rho + \mathrm{i})|A|^2 A \tag{2}$$

where t is the dimensionless time and $x \in [0, 2\pi]$ is the spatial variable. The parameters q, ρ and c_0 are taken to be real and positive and the Newell criterion [15] for modulational instability is assumed, $\rho c_0 < 1$. This implies there will always exist values of q at which the homogeneous solution to equation (2) is unstable.

For fixed ρ and c_0, q is the control parameter. As q is decreased, a sequence of bifurcations occurs, whose exact form depends on the imposed boundary conditions. For sufficiently small q *turbulence*, defined here as the presence of chaos in both time and space series, can occur in solutions of (2). Temporal chaos is indicated by sensitivity to initial conditions (i.e., at least one positive Lyapunov exponent) or a broad band frequency spectrum, while spatial chaos is indicated by a broad band wavenumber spectrum. The turbulent regimes which occur when q is small are the focus of the present study. We note that the parameter regions which we consider for (2) are generally far from criticality and hence not of direct physical relevance.

Most of the numerous studies of the 1-D CGL equation which have been undertaken have concentrated on solution bifurcations and the transition to chaotic behaviour [13, 16–20]. Some work has been done on the behaviour in chaotic regimes far from criticality [10, 21–23], using $\rho, c_0 \sim 1$ and $q \ll 1$. However, length-scale arguments presented in [10] suggest that interesting behaviour might occur for $c_0 \ll 1$ when q is small. In addition, recent analytical results [1, 24, 25] suggest that $\rho, c_0 \ll 1$ is an important case to study for $q \ll 1$. We note that results for the scaling of certain quantities in this last case have very recently appeared [26].

Sirovich, Rodriguez and Knight [10] studied (2) subject to Dirichlet boundary conditions, $A(0, t) = A(\pi, t) = 0$. Taking $\rho = c_0 = 0.25$, they obtained the bifurcation sequence for $0.08 \leqslant q \leqslant 1.0$ via numerical simulations. For sufficiently small q, both spatial and temporal chaos occurred, the attractor dimension increased linearly with $1/q$, and the wavenumber spectrum exhibited a universal form. Employing length-scale arguments similar to those used in fluid mechanics, Sirovich *et al* derived the correct behaviour in both the energy-bearing and dissipative portions of the wavenumber spectrum.

Bartuccelli, Constantin, Doering, Gibbon and Gisselfalt [1, 24, 25] performed an analytical study of the CGL equation, assuming fully periodic boundary conditions. They examined the way in which the q-dependence of various quantities change as ρ and c_0 become small. This case of $\rho, c_0 \ll 1$ is the *dissipationless* limit, since for $\rho = c_0 = 0$ the CGL equation becomes the (conservative) nonlinear Schrödinger (NLS) equation. Asymptotic bounds obtained by Bartuccelli *et al* suggest that large intermittent fluctuations can occur in 2-D and 3-D near the dissipationless limit. However, their results imply that in 1-D only small deviations from mean quantities are possible.

Generally, turbulence is termed strong or 'hard' when it displays large fluctuations from mean quantities, and termed weak or 'soft' when it does not. Therefore, the results of Bartuccelli *et al* imply that only soft turbulence can occur in the 1-D CGL equation. One common criterion for distinguishing between soft and hard turbulence, which will be used below, is the form of the probability density functions. As discussed by Heslot *et al* [27] and Castaing *et al* [28] in the context of Rayleigh–Bénard convection, soft turbulence is characterized by purely Gaussian p.d.f.'s, while the presence of hard turbulence is indicated by p.d.f.'s with exponential tails. Another important characteristic of high Reynolds number fluid turbulence, which we might expect in solutions of (2) when $c_0 \ll 1$, is the presence of a range of wavenumbers intermediate to the energy-bearing and dissipative ranges. In this 'inertial' range, both energy production and dissipation are relatively unimportant, hence the dominant process is the transfer of energy from low to high wavenumber modes.

Motivated by the ideas discussed above, we have made a numerical investigation of

the 1-D CGL equation (2) subject to Dirichlet boundary conditions when c_0 (and hence the dissipation $q^2 c_0$) is small. A split-step method recently presented for the CGL equation [29] was used to obtain approximate solutions to (2) in the subspace of the sine modes. A sine expansion is sufficient because the CGL equation respects parity symmetries.

Briefly, our numerical method involves splitting (2) into the two exactly solvable equations

$$\frac{\partial A^{(1)}}{\partial t} = q^2(c_0 + \mathrm{i})\frac{\partial^2 A^{(1)}}{\partial x^2} \tag{3}$$

and

$$\frac{\partial A^{(2)}}{\partial t} = \rho A^{(2)} - (\rho - \mathrm{i})A^{(2)}|A^{(2)}|^2. \tag{4}$$

For Dirichlet boundary conditions, (3) is solved by the 'diffusion solution'

$$A^{(1)}(x, t) = \sum_{k=0}^{\infty} f_k^{(1)}(0)\exp[-k^2 q^2(c_0 + \mathrm{i})t]\,\sin kx, \tag{5}$$

where $f_k^{(1)}(0)$ is the kth Fourier coefficient of $A^{(1)}(x, 0)$. Equation (4) is solved by the 'nonlinear solution'

$$A^{(2)}(x, t) = \frac{R(x, 0)\, e^{\rho t}}{\sqrt{1 - R^2(x, 0) + R^2(x, 0)\, e^{2\rho t}}} \tag{6}$$
$$\times \exp\{\mathrm{i}[\Theta(x, 0) + \frac{1}{2\rho}\log(1 - R^2(x, 0) + R^2(x, 0)\, e^{2\rho t})]\},$$

where $R(x, 0)$ and $\Theta(x, 0)$ are the magnitude and phase, respectively, of $A^{(2)}(x, 0)$. Once the solutions (5) and (6) have been discretized in space and time, they can be used to construct an efficient numerical scheme for (2) which has spectral accuracy in space and second-order accuracy in time [29].

For each set of parameters, we chose a number of sine modes N, based on preliminary experiments, such that the energy in the highest modes would be very small (e.g., $|f_N|/|f_1| \sim 10^{-7}$). We then checked that there were no significant aliasing errors by a comparison with the wavenumber spectrum obtained for $N' = 2N$. Generally, we used a spatial resolution of at least $N = 255$ (which was used for all cases $q = 0.05$) and a time step $\Delta t \sim 10^{-4}$–10^{-3}. To obtain the results reported here, we initiated all simulations with $A(x, 0) = 0.02(1 + \mathrm{i})\sin x$. We then began detailed observations of the chaotic solutions after the system evolved to a statistically steady state, which typically required several hundred time units. The main result of our simulations, determined from the Gaussian form of the probability density functions, is that for both $c_0 \downarrow 0$, ρ fixed and $\rho = c_0 \downarrow 0$ only soft turbulence occurs. A related result is that an inertial range does not appear in either of these limits.

In section 2 we present results, including wavenumber and frequency spectra and p.d.f.'s, for $c_0 \downarrow 0$, $\rho = 0.25$. In the next three sections, beginning with the power spectra and p.d.f.'s in section 3, we concentrate on the dissipationless limit $\rho = c_0 \downarrow 0$. In section 4 we discuss estimates of the dimension of the inertial manifold and the attractor dimension, and in section 5 we present results on universality in the dissipationless limit. Additional remarks on the observed wavenumber spectra are given in section 6, and in section 7 the main conclusions are summarized.

Results of simulations of the 2-D CGL equation near the dissipationless limit, which we have also performed, are forthcoming [30].

2. A low dissipation limit: $c_0 \downarrow 0$

For $\rho = c_0 = 0.25$, solutions of the 1-D CGL equation (2) under Dirichlet boundary conditions exhibit turbulence for $q < 0.21$ [10]. The spatial disorder which occurs can be seen in figure 1. As demonstrated in [10], both analytically and numerically, as $q \downarrow 0$ the averaged wavenumber spectra of these turbulent solutions all take the same universal form for $\rho, c_0 \sim 1$. Two distinct ranges occur: an integral range, in which $\langle |f_k|^2 \rangle \simeq$ constant, and a dissipative range, in which $\langle |f_k|^2 \rangle \sim e^{-qk}(qk)^{-4}$, where $\langle \cdot \rangle$ represents a time average. Confirmation of this is indicated in figure 2 where, as in the rest of this paper, wavenumber spectra were computed by taking a time average over several thousand time units.
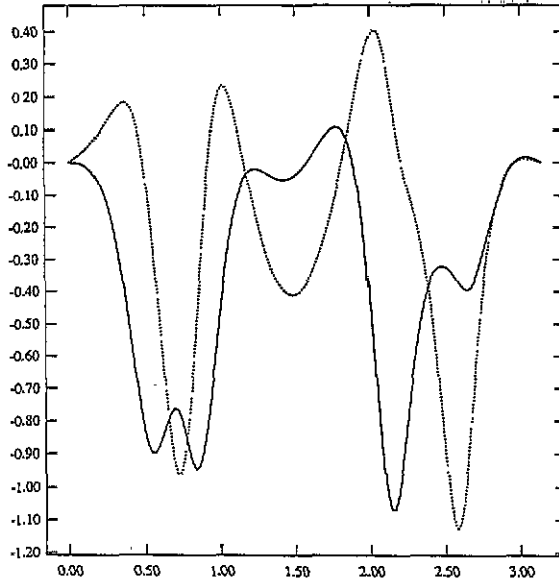

Figure 1. Snapshot of A showing the spatial chaos which occurs for $q = 0.1$, $\rho = c_0 = 0.25$. For a fixed time t we plot the real (—) and imaginary ($\cdots$) parts of A as functions of x.

The existence of two ranges in the universal spectrum is a consequence of dimensional arguments. All quantities in (2) except x and q are dimensionless, thus all relevant length scales necessarily involve q. One scale is the dissipation length scale $\delta_d \equiv q\sqrt{c_0}$ [10]. For $k \ll k_d \equiv 1/\delta_d$, dissipation is small, whereas for $k \geqslant k_d$ (the dissipative range) it is moderate to large.

A second length scale can be derived from an analysis of the thickness of the boundary layer which is produced by imposing boundary conditions [10]. This scale equals the magnitude of the diffusion coefficient, $q(1 + c_0^2)^{1/4}$, and is designated δ_c. Because the dynamics at points outside the boundary layer are essentially independent of the boundary conditions, δ_c is taken to be a measure of correlation. Assuming points separated by distances greater than δ_c are uncorrelated specifies universal behaviour for $k \leqslant 1/\delta_c$ (the integral range).

In [10] universality was verified down to $q = 0.01$ using $\rho = c_0 = 0.25$, and no other behaviour was found. But when $c_0 \sim 1$, we have $\delta_c \simeq \delta_d$, so the two length scales are not expected to be well separated. This suggests that for $c_0 \ll 1$ there might be an intermediate range of wavenumbers between the integral and dissipative ranges, perhaps an inertial range.

The possibility of an inertial range was considered for $c_0 \downarrow 0$ when $q = 0.1$ and
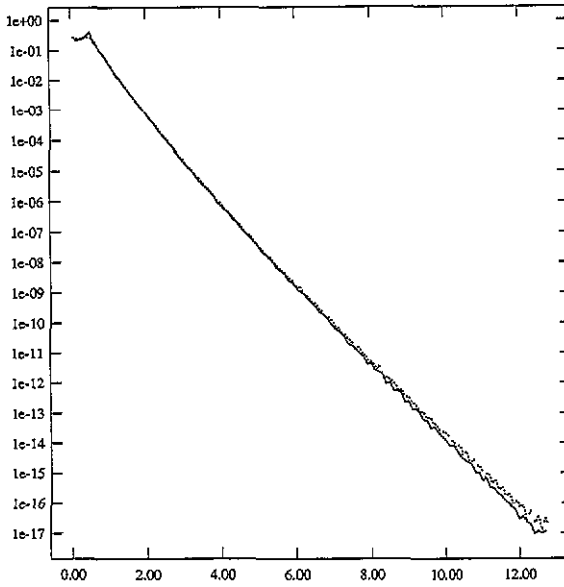
Figure 2. Wavenumber spectra showing the universal form for $\rho = c_0 = 0.25$. For $q = 0.1$ (—) and $q = 0.05$ ($\cdots$) we plot $\log[\langle|f_k|^2\rangle/q]$ versus qk.

$\rho = 0.25$. From the spectra for $c_0 = 10^{-2}$, 10^{-3} and 10^{-4}, shown in log–log form in figure 3, it can be seen that no inertial range appeared. The transitional region between the integral and dissipative ranges flattened slightly and its boundaries steepened as c_0 was decreased but, contrary to what would be expected for a true inertial range, its extent did not increase significantly as the dissipation was decreased.
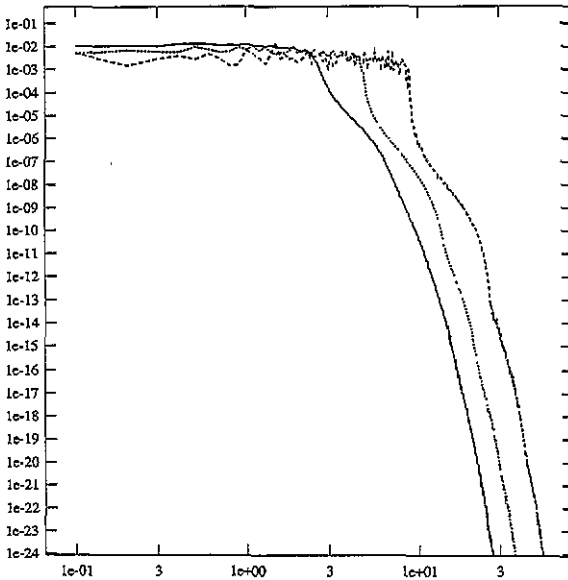
Figure 3. Wavenumber spectra for $c_0 = 10^{-2}$ (—), 10^{-3} ($\cdots$) and 10^{-4} (- - -), when $\rho = 0.25$ and $q = 0.1$. Here we plot $\log\langle|f_k|^2\rangle$ as a function of $\log qk$.

A point to note is that if the smallest scale to be resolved is δ_d, then it should be

necessary, for example, to take $N \simeq 4\pi/\delta_d = O(10^4)$ points for $q = 0.1, c_0 = 10^{-4}$. However, using the criteria discussed in the introduction, it was found experimentally that far fewer points (~ 300) are actually needed to accurately solve the problem. This is demonstrated by the sharp fall-off of all three wavenumber spectra in figure 3 for $k \geqslant 100$. This result indicates that the smallness of length scales is strongly limited by their production as well as by their dissipation.

Another important point is that as c_0 was decreased with q and ρ fixed, the numerically observed boundary of the integral range, denoted k_I, moved significantly to higher wavenumbers. This should not have occurred if δ_c controls the size of the integral range, because as c_0 decreases from $1/4$ to 0, δ_c remains approximately equal to q.

To help explain these results, as well as those to follow, we consider the linearized version of (2) in Fourier space,

$$\frac{\mathrm{d}\, f_k}{\mathrm{d}t} = -q^2 k^2 (c_0 + \mathrm{i}) f_k + \rho f_k. \tag{7}$$

This shows growth for $k^2 < \rho/(q^2 c_0)$ and decay for $k^2 > \rho/(q^2 c_0)$, suggesting a sharp change in behaviour near $k = k_L \equiv q^{-1}\sqrt{\rho/c_0}$. Modes with wavenumbers less than k_L are linearly unstable and, in addition to participating in nonlinear energy exchanges, can be expected to be dynamically self-sustaining. On the other hand, since for individual modes the nonlinear term in (2) acts to limit growth, modes with wavenumbers greater than k_L are not self-sustaining and only exist through a net influx of energy from other modes. These ideas about k_L explain the increase in k_I in the numerical experiments, where c_0 was decreased with q and ρ fixed, since $k_L \propto c_0^{-1/2}$ is expected to be the boundary between the energy-bearing modes and those dominated by dissipation.

Another effect found for $c_0 \downarrow 0$ is that higher temporal frequencies appeared as c_0 was decreased. This can be seen in the frequency spectra in figure 4, which were computed by averaging over segments of data taken from a long time series. It is thought that the increase in the highest physically relevant frequency is related to the increase in k_I, since the complex diffusivity in (2) associates with each Fourier mode k an angular frequency $q^2 k^2$.

Probability density functions for $c_0 \downarrow 0$ are shown in figure 5. It can be seen that these p.d.f.'s are Gaussian, implying there are no unusually large deviations. Only soft turbulence is observed for the 1-D CGL equation (2) in the limit $c_0 \downarrow 0$ with q and ρ fixed.

3. The dissipationless limit: $\rho = c_0 \downarrow 0$

A problem in the low dissipation limit $c_0 \downarrow 0$, made clear by the discussion of k_L, is that as the characteristic wavenumber of dissipation increases, so does the characteristic integral wavenumber. Thus in this limit the two scales may not become sufficiently separated for an inertial range to appear. To resolve this issue we can study the limit $\rho = c_0 \downarrow 0$, q fixed, in which (2) becomes the NLS equation

$$\frac{\partial A}{\partial t} = \mathrm{i}q^2 \frac{\partial^2 A}{\partial x^2} + \mathrm{i}|A|^2 A. \tag{8}$$

Thus the limit $\rho = c_0 \downarrow 0$ is a special case of the dissipationless limit $\rho, c_0 \downarrow 0$ and therefore is appropriate for investigating the low dissipation behaviour of the CGL equation.
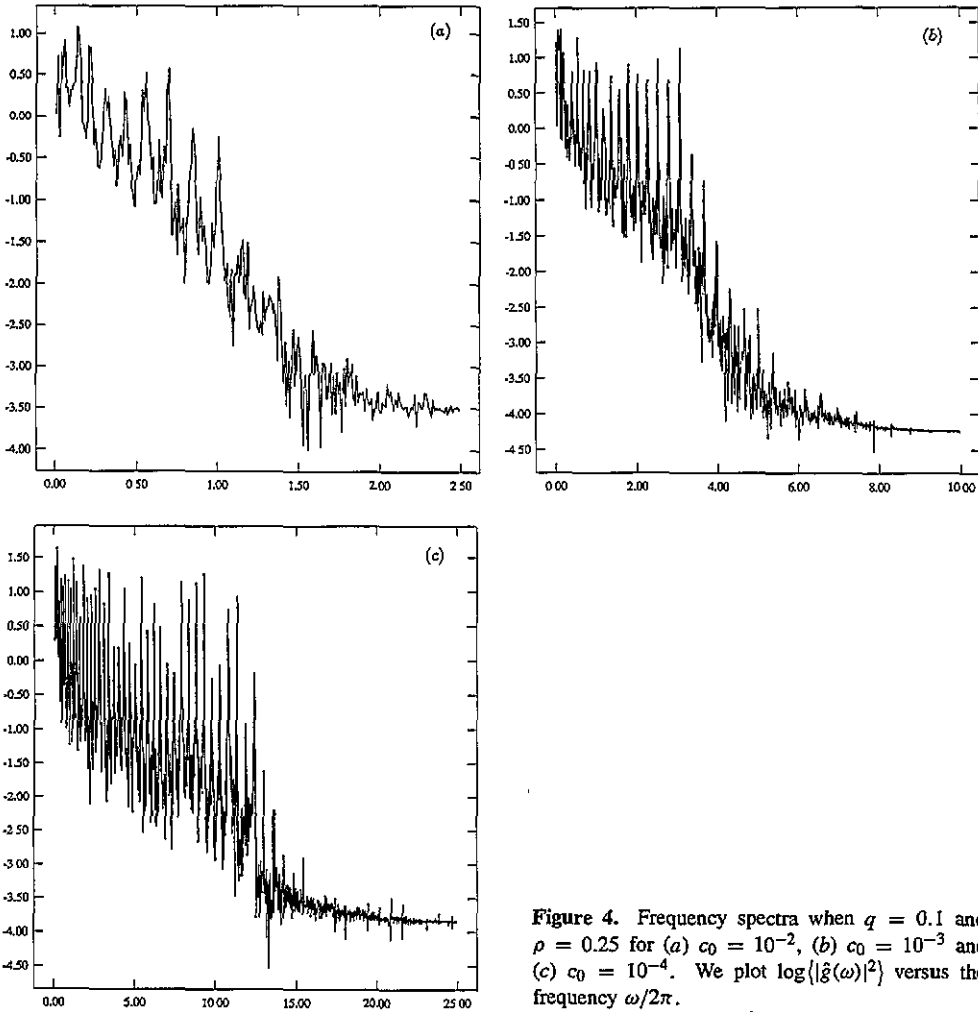
Figure 4. Frequency spectra when $q = 0.1$ and $\rho = 0.25$ for (a) $c_0 = 10^{-2}$, (b) $c_0 = 10^{-3}$ and (c) $c_0 = 10^{-4}$. We plot $\log\{|\hat{g}(\omega)|^2\}$ versus the frequency $\omega/2\pi$.

3.1. Wavenumber spectra

With the preceding discussion in mind, numerical simulations were performed on (2) for $q = 0.1$ and $\rho = c_0 \leqslant 0.25$. Figure 6(a) shows the wavenumber spectrum when $\rho = c_0 = 0.01$ and, for comparison, the spectrum when $\rho = c_0 = 0.25$, both for $q = 0.1$. It can be seen that for $\rho = c_0 = 0.01$ the drop-off in the dissipative range is less steep than for $\rho = c_0 = 0.25$. This is as expected since δ_d is smaller for the $\rho = c_0 = 0.01$ case. It can also be seen that the behaviour of the low wavenumber modes is different for the two cases. From a close-up of the low wavenumber portion of figure 6(a), shown in figure 6(b), it appears that in the integral range $\langle|f_k|\rangle$ is nearly constant for $\rho = c_0 = 0.25$ but decreases with increasing k for $\rho = c_0 = 0.01$. It can be seen that k_{I} is larger for $\rho = c_0 = 0.01$ and that a transitional region appears in the range $1.00 \leqslant qk \leqslant 1.25$. However, there is no true inertial range. As $\rho = c_0$ is decreased further, first to 10^{-3} and then to 10^{-4}, wavenumber spectra remain nearly identical to that found for $\rho = c_0 = 0.01$. These results are shown in figure 7. There is no further increase in k_{I}, and the only effect seen for $0 < \rho = c_0 < 0.01$ is the continued decrease of the decay rate in the dissipative range.
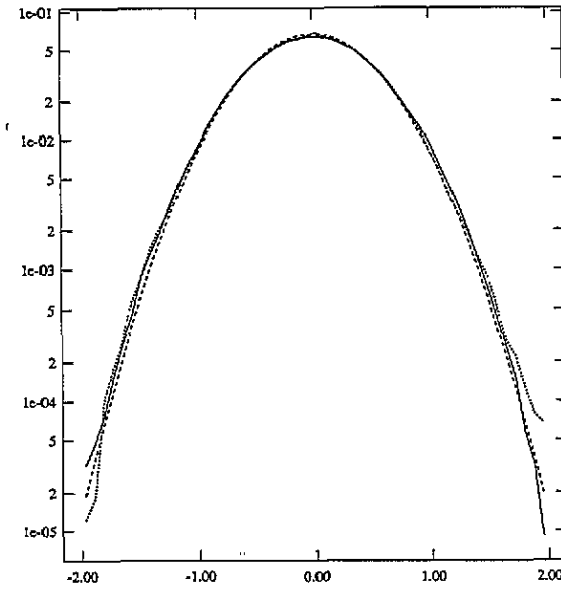
Figure 5. Probability density functions for $c_0 = 10^{-3}$ (—) and $c_0 = 10^{-4}$ ($\cdots$), when $\rho = 0.25$ and $q = 0.1$. We plot $\log P(A_r = s)$ versus s, where $P(A_r = s)$ is the probability that the real part of A is approximately equal to s. For comparison, we also plot the parabola $-2.03s^2 - 2.71$ (- - -).
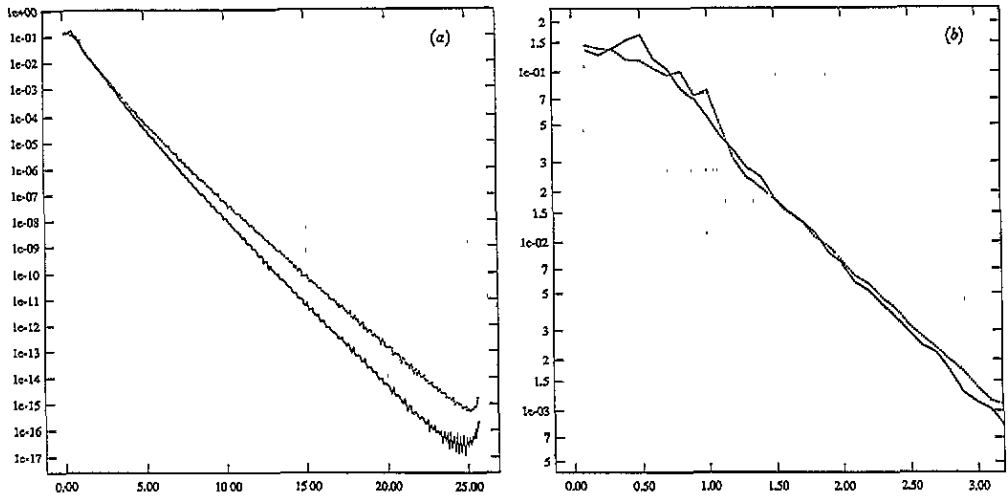

Figure 6. Wavenumber spectra for $\rho = c_0 = 0.01$ ($\cdots$) and $\rho = c_0 = 0.25$ (—), when $q = 0.1$. We plot the logarithm of $\langle |f_k| \rangle$ against the normalized wavenumber qk (a) for the full range of k, (b) for $qk \leqslant 3$.

These results indicate that the extent of the integral range is in fact controlled by k_L. Once k_L and k_d become well separated, the integral range becomes as large as possible, given q and $\rho = c_0$. In other words, as $\rho = c_0 \downarrow 0$, $k_I \uparrow k_L$. For fixed q, the above results also indicate that, except at very high k, the wavenumber spectra quickly converge to a single curve. Given the results shown in figure 7, it is now assumed that the dissipationless limit $\rho = c_0 \downarrow 0$ is well described by the case $\rho = c_0 = 0.01$.

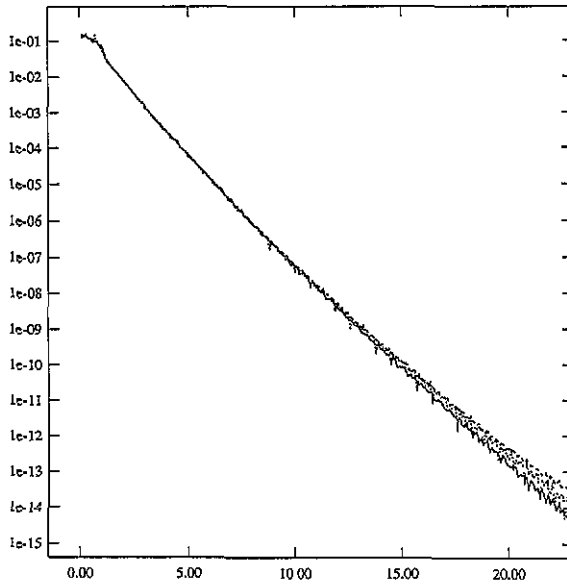To better understand the wavenumber spectrum near the dissipationless limit, we seek

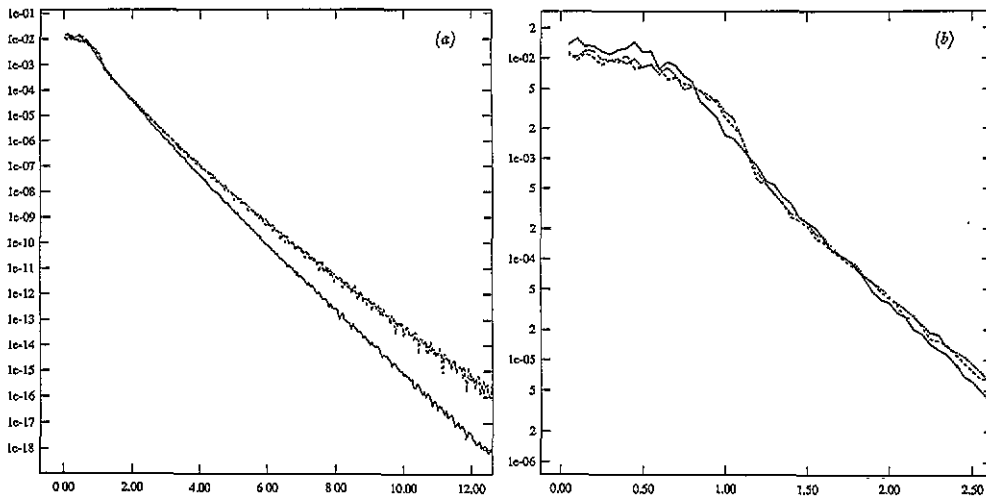**Figure 7.** Wavenumber spectra for $\rho = c_0 = 10^{-2}$ (—), 10^{-3} ($\cdots$) and 10^{-4} (- - -), when $q = 0.1$. We plot $\log \langle |f_k| \rangle$ versus qk.

Figure 8. Wavenumber spectra for $\rho = c_0 = 0.25$ (—), 0.01 ($\cdots$) and 0.001 (- - -), when $q = 0.05$. We plot $\log \langle |f_k|^2 \rangle$ versus qk (a) for the full range of k, (b) for $qk \leqslant 2.5$.

a larger integral range than occurs for $q = 0.1$. Therefore, simulations were performed on (2) for $0.25 \leqslant \rho = c_0 \leqslant 10^{-3}$ when $q = 0.05$. Examination of the $q = 0.05$ wavenumber spectra for $\rho = c_0 \downarrow 0$, given in figure 8(a), gave qualitatively the same result as for $q = 0.1$. Figure 8(b), a close-up of the integral ranges in figure 8(a), shows that for $\rho = c_0 \ll 1$ we have $\langle |f_k|^2 \rangle \simeq$ constant for approximately the first ten wavenumbers ($qk \leqslant 0.5$), just as it is for $\rho = c_0 = 0.25$. This suggests that the correlation length arguments used in [10] to derive the universal form of the integral range for $\rho, c_0 \sim 1$ continue to be valid near the dissipationless limit. However, as figure 8(b) shows, since these arguments require $k < O(1/\delta_c)$, they do not apply throughout the full, dissipationless integral range. As a final

demonstration that no inertial range occurs, a log–log plot of the wavenumber spectrum for $q = 0.05$, $\rho = c_0 = 10^{-3}$ is shown in figure 9.
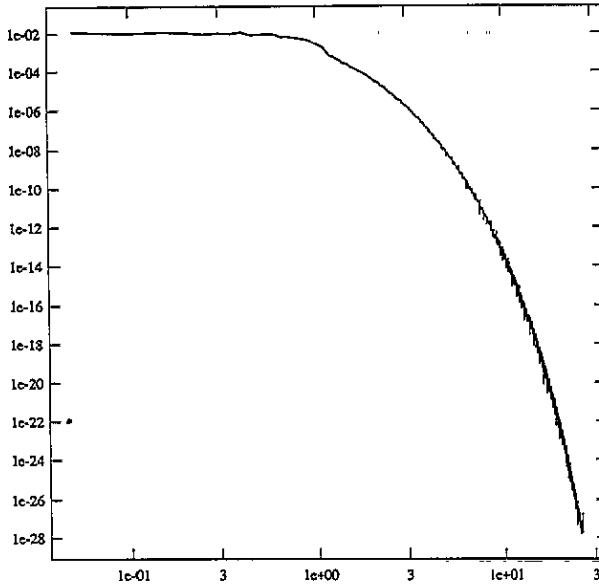

Figure 9. Wavenumber spectrum for $q = 0.05$, $\rho = c_0 = 10^{-3}$. Here we plot $\log\langle |f_k|^2 \rangle$ versus $\log qk$.

The modifications near the dissipationless limit to the wavenumber spectrum derived in [10] for $\rho, c_0 \sim 1$ have now been described. These modifications have been explained by using the wavenumber scale k_L, in addition to the length scales δ_c and δ_d.

3.2. Frequency spectra and correlation functions

Frequency spectra were computed for $\rho = c_0 = 0.25$ and $\rho = c_0 = 0.01$ when $q = 0.05$. This was done by averaging the frequency spectrum at each grid point, $|\hat{g}(x_j, \omega)|^2$, over all $j = 1, 2, \ldots, N$. As figure 10 shows, the fall-off becomes exponential at high frequencies, as expected from theoretical considerations, and no dramatic changes occur in the dissipationless limit.

From the wavenumber and frequency spectra presented above, one can directly calculate correlation functions. This was done for $\rho = c_0 = 0.25$ and $\rho = c_0 = 0.01$, using $q = 0.05$. The temporal correlations in figure 11(*a*) show that there is actually a slight *increase* in the largest physically relevant time scale as the dissipationless limit is approached. The spatial correlations in figure 11(*b*) give a slight decrease in the correlation length near the dissipationless limit, from $l_c = 0.27$ for $\rho = c_0 = 0.25$ to $l_c = 0.24$ for $\rho = c_0 = 0.01$. The observed decrease in the correlation length is small (7.4%), but still larger than the 1.5% decrease predicted by $\delta_c = q(1 + c_0^2)^{1/4}$. Thus the assumption that δ_c is a measure of the correlation length [10] is seen to be an approximation.

3.3. Probability density functions

We now consider the prediction in [1] that large variations from spatial and temporal averages do not occur near the dissipationless limit of the 1-D CGL equation. Since
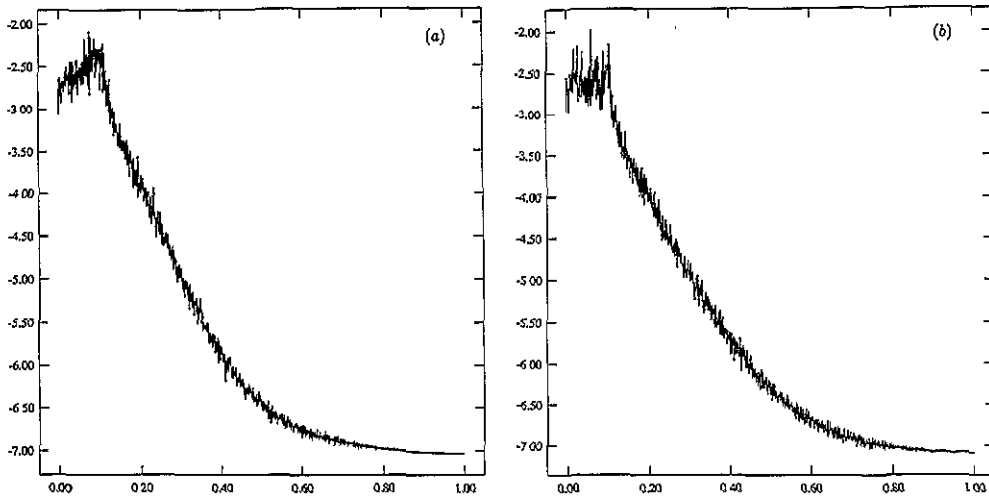
Figure 10. Frequency spectra when $q = 0.05$ for (a) $\rho = c_0 = 0.25$, (b) $\rho = c_0 = 0.01$. We plot $|\hat{g}(\omega)|^2$ versus the frequency $\omega/2\pi$.
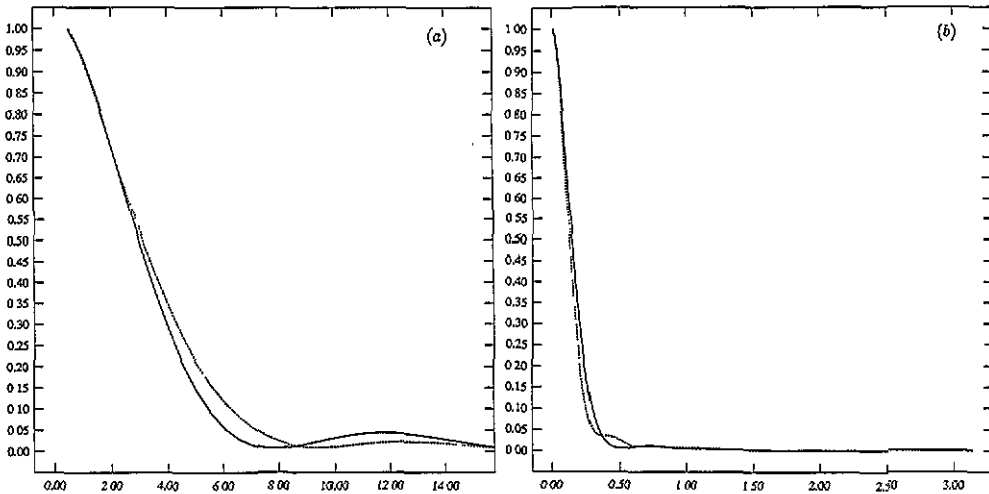

Figure 11. Correlation functions when $q = 0.05$ for $\rho = c_0 = 0.25$ (—) and $\rho = c_0 = 0.01$ ($\cdots$): (a) temporal correlation $C(t)$, (b) spatial correlation $C(x)$.

the determination of hard or soft fluid turbulence is often made using probability density functions, we calculated p.d.f.'s for $\rho = c_0 = 0.25$ and $\rho = c_0 = 0.01$ when $q = 0.05$.

As can be seen from the profile in figure 12 of the time-averaged squared magnitude, $\langle |A(x, t)|^2 \rangle$, Dirichlet boundary conditions produce boundary layers at $x = 0$ and $x = \pi$. In order that all points used to obtain the p.d.f.'s be nearly equivalent, only points at least a distance of $\pi/10$ from the 'boundaries' were used. The p.d.f.'s were constructed by sampling the real part of $A(x, t)$ at these interior points at a series of uncorrelated times, the same procedure used to obtain the p.d.f.'s for $c_0 \downarrow 0$, $\rho = 0.25$. As figure 13 shows, the p.d.f.'s for $\rho = c_0 = 0.25$ and $\rho = c_0 = 0.01$ are similar, indicating no dramatic change in behaviour near the dissipationless limit. Also, both p.d.f.'s are essentially Gaussian, implying there are no large deviations in A_r. In particular, the result for $\rho = c_0 = 0.01$ implies that hard turbulence does not occur near the dissipationless limit of the 1-D CGL
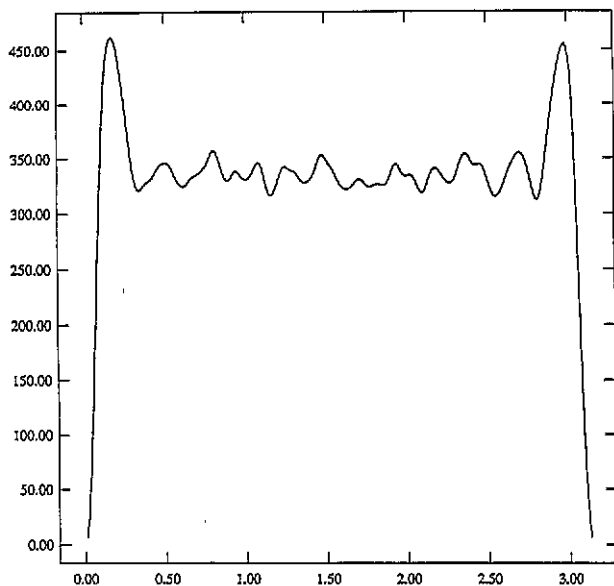
Figure 12. Graph of time-averaged squared magnitude of A showing the effect of the boundary conditions. For $q = 0.05$ and $\rho = c_0 = 0.01$, we plot $\langle |A(x, t)|^2 \rangle$ versus x.

equation.
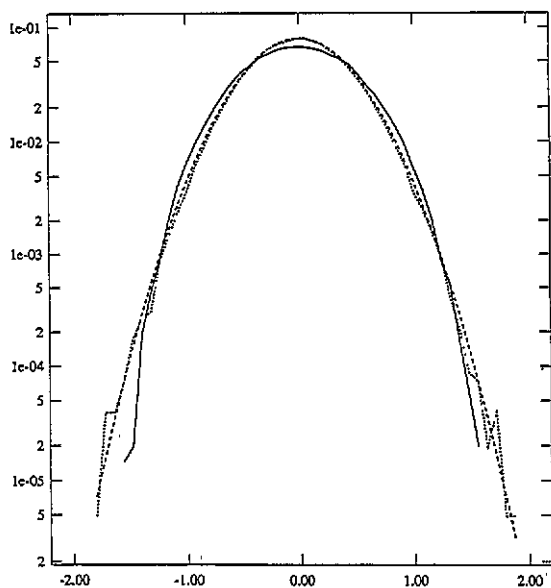
Figure 13. Plots of the probability density functions for $\rho = c_0 = 0.25$ (——) and $\rho = c_0 = 0.01$ ($\cdots$) when $q = 0.05$. We plot $\log P(A_r = s)$ and the parabola $-2.87s^2 - 2.54$ (- - -).

Remark. Including points near the boundaries does not change the above results. The logarithm of the p.d.f. for $\rho = c_0 = 0.01$, $q = 0.05$, computed using all spatial points, is fit almost exactly by a parabola of the form $-as^2 + b$. This confirms the finding of soft turbulence.

4. Other characteristics in the dissipationless limit

The results presented in section 3 confirm the general prediction of soft turbulence made by Bartuccelli *et al* in [1]. We now examine their results in greater detail and make some quantitative comparisons with our numerical results for $\rho = c_0 = 0.01$.

Bartuccelli *et al* have studied the following form of the complex Ginzburg–Landau equation:

$$\frac{\partial A(x, t)}{\partial t} = (1 + i\nu)\nabla^2 A(x, t) + RA(x, t) - (1 + i\mu)|A(x, t)|^2 A(x, t) \quad (9)$$

where ∇^2 is the d-dimensional Laplacian with $d = 1, 2$ or 3. They assume arbitrary initial conditions and periodic boundary conditions on $[0, 1]^d$ and take R to be large.

The connection between equation (2) and equation (9) for $d = 1$ is given by the parameter relations

$$R = 4\pi^2 \frac{\rho}{q^2 c_0} \qquad \nu = \frac{1}{c_0} \qquad \mu = \frac{-1}{\rho} \quad (10)$$

and the variable relations

$$x' = \frac{1}{2\pi} x \qquad t' = \frac{1}{4\pi^2} q^2 c_0 t \qquad A' = 2\pi \sqrt{\frac{\rho}{q^2 c_0}} A \quad (11)$$

where $'$ denotes the variable in equation (9).

Remark 1. The above relations imply that the L^2 norms obey $||A'||_2^2 \sim R||A||_2^2$, while Bartuccelli *et al* give the uniform bound $\langle ||A'||_2^2 \rangle \leqslant R$. We have found that $\langle ||A||_2^2 \rangle$ varies only slightly with q, ρ and c_0, which is consistent with the above analytical result. Further, although we have not measured the asymptotic maximum of $||A||_2^2$, our observations suggest it does not deviate substantially from the mean.

Remark 2. For a quintic nonlinearity and fixed, small–dissipation values of μ and ν, Luce and Doering [26] found that both $\limsup_{t\to\infty} ||A'||_2^2$ and $\limsup_{t\to\infty} ||A'||_\infty^2$ scaled as $R^{1/2}$. This suggests that the behaviour of these quantities is related to the rescaling one obtains for (9) in the quintic case, $A' = \sqrt{2\pi}(\frac{\rho}{q^2 c_0})^{1/4} A = R^{1/4} A$.

It can be seen that the condition for modulational instability, $0 < \rho c_0 < 1$, is equivalent to $\mu\nu < -1$, implying the regions of interest are in the second and fourth quadrants of the μ–ν plane. The dissipationless limit for (9) is defined as $|\nu|, |\mu| \to \infty$ with $\nu\mu < 0$. Since ρ and c_0 have been assumed to be positive, ν and μ will be taken to be positive and negative, respectively, giving a direct correspondence between the dissipationless limits $\rho = c_0 \downarrow 0$ and $-\mu = \nu \uparrow \infty$. We note that $q = 0.05$, $\rho = c_0 = 0.01$ corresponds to $R \simeq 15,791$.

It is known that in 1-D the NLS equation has an infinite number of conserved quantities, whereas in 2-D and 3-D blow-up singularities can occur in finite time (see [24, 31]). In [1], the relationship between the CGL and NLS equations was used as the main basis for deriving bounds on various quantities related to (2) throughout the μ–ν plane. We now discuss our numerical results for three of these quantities: the dimension of the inertial manifold $d_{\text{i.m.}}$, the attractor dimension d_{att}, and the Lyapunov functional F_2. First, however, we deal with the important issue of the relation of our numerics to the global dynamics of (2).

For $\rho = c_0 = 0.25$ and small q, the numerical studies of Keefe [22] and Sirovich *et al* [10] found only a single attractor for periodic, Neumann, or Dirichlet boundary conditions.

Thus, there is reason to believe that the single attractor found in the present study for each set of parameters in the range $\rho = c_0 \leqslant 0.6$, $q \leqslant 0.1$ is the only one for (2). This idea is further supported by recent results [11, 23] which indicate that for periodic boundary conditions and small q there is a single global attractor for $\rho = c_0 \lesssim 0.8$. In addition, when q is small (which corresponds to a long domain—see section 5) one expects that the results will not depend on the boundary conditions and, in particular, that numerics done for Dirichlet boundary conditions will be relevant to estimates derived assuming periodic boundary conditions. Evidence for this is the fact that for all three boundary conditions studied in [22] and [10], the attractor dimension showed the same behaviour ($d_{\text{att}} \sim 1/q$) for sufficiently small q. We therefore conclude that our numerical results for various quantities, such as $d_{\text{i.m.}}$ and d_{att}, should be relevant to the global bounds obtained by Bartuccelli *et al*.

4.1. Estimates of the dimension of the inertial manifold

A quantity of interest in exploring the behaviour of (2) near the dissipationless limit is the dimension of the inertial manifold, i.e., the theoretical number of basis functions needed to describe solutions. As discussed in [1] this number, denoted $d_{\text{i.m.}}$, is generally expected to be much greater than the attractor dimension d_{att}. Here we seek to determine the dependence of $d_{\text{i.m.}}$ on the parameters in (2), particularly on q for $\rho = c_0 \ll 1$.

Wavenumber spectra provide a measure of the number of significant Fourier modes contained in solutions of (2). An examination of the spectra for $q = 0.1$ and $q = 0.05$ when $\rho = c_0$ suggests this number is proportional to k_{I}, which was shown to reach the limiting value $k_{\text{L}} = 1/q$ for $\rho = c_0 \leqslant 0.01$. From figure 8 it can be seen that when $q = 0.05$ we have $k_{\text{I}} \simeq 10$ for $\rho = c_0 = 0.25$ and $k_{\text{I}} \simeq 20$ for $\rho = c_0 = 0.01$. Using k_{I} to estimate the number of Fourier modes needed to describe solutions, however, neglects all the dissipative-range modes. Another estimate can be obtained by looking at the number of Fourier modes required to capture a certain percentage of the total, time-averaged energy, defined as

$$E_{\text{av}} = \frac{1}{2\pi} \int_0^{2\pi} \langle |A(x,t)|^2 \rangle \, dx \simeq \frac{1}{2} \sum_{k=1}^{N} \langle |f_k|^2 \rangle. \tag{12}$$

Using 99% as the cutoff implies that, when $q = 0.05$, we need 27 Fourier modes for $\rho = c_0 = 0.25$ and 29 for $\rho = c_0 = 0.01$. Using so few modes may not give acceptable results, but these estimates give a better idea than does k_{I} of the overall change in the distribution of energy in the wavenumber spectrum as the dissipationless limit is approached.

The above discussion suggests that the 'Fourier dimension' of the problem may not increase very much as the dissipationless limit is approached. In order to examine this idea, two different types of measures of the Fourier dimension, d_{F}, were computed. The first is the number of modes required to get a certain amount of drop-off in the wavenumber spectrum from its peak value. The second type of measure used was the one discussed above, i.e., the number of modes required to capture a certain percentage of the energy of the system.

Of interest is the q-dependence of d_{F} near the dissipationless limit. Figure 14 shows the results of several estimates of the Fourier dimension obtained from the wavenumber spectra for $\rho = c_0 = 0.01$. It was found that over the range of q studied, the Fourier dimension of (2) near the dissipationless limit increases linearly with $1/q$. The data in table 1 shows that for the two most stringent measures used we have $q d_{\text{F}} \simeq$ constant over the range studied. If the d_{F}'s calculated above are taken to be estimates of the dimension of the inertial manifold, then there is a lack of agreement with the predictions in [1] for the 1-D dissipationless limit.
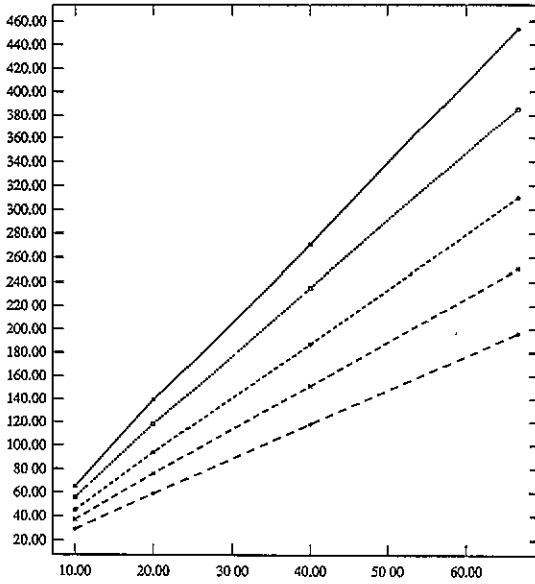
Figure 14. Various estimates of the Fourier dimension for $\rho = c_0 = 0.01$. We plot, as functions of $1/q$, the number of Fourier modes required to obtain a drop-off in the wavenumber spectrum of 10^{-7} ($\cdots\square\cdots$) and 10^{-8} (—■—), and the number required to capture all but 10^{-2} (- -◇- -), 10^{-3} (- -×- -) and 10^{-4} (- -○- -) percent of the time-averaged energy of the system.

Table 1. Estimates of the Fourier dimension, d_F, obtained using the 10^{-8} drop-off and $10^{-4}\%$ energy error criteria for the case $\rho = c_0 = 0.01$.

q	10^{-8} drop-off			$10^{-4}\%$ energy error		
	d_F	$q d_F$	$q^2 d_F$	d_F	$q d_F$	$q^2 d_F$
0.1	65	6.5	0.6500	45	4.5	0.4500
0.05	139	6.95	0.3475	94	4.7	0.2350
0.025	271	6.775	0.1694	187	4.675	0.1169
0.015	453	6.795	0.1019	310	4.65	0.0698

For $\rho = c_0$ these bounds imply that $d_{i.m.} \leqslant cq^{-2}$, which is seen to be an overestimate of the results in table 1.

Next we examine the behaviour of the Fourier dimension for $\rho = c_0 \downarrow 0$. An analysis of wavenumber spectra computed for $q = 0.05$ and $0.6 \leqslant \rho = c_0 \leqslant 10^{-3}$ shows that d_F increases only slightly as $\rho = c_0$ is decreased and becomes nearly constant in the dissipationless limit. While δ_d decreases by a factor of more than twenty, d_F only increases by approximately 50%. Thus, the idea that the dissipation length scale determines the number of Fourier modes required to accurately describe the physics of the problem does not strictly apply to (2), and we conclude that the occurrence of small length scales is limited more by their production than by dissipation.

Remark. Since $d_{i.m.}$ is defined as the number of basis functions needed to completely describe the behaviour on the attractor, one expects that d_F underestimates the actual value of $d_{i.m.}$. However, since our simulations were well-resolved and very small energy-error criteria were used to compute d_F, we expect that $d_{i.m.} \propto d_F$. Therefore, d_F should accurately

represent the behaviour of $d_{i,m}$. with respect to changes in the parameters in (2).

Another estimate of the number of functions needed to describe solutions of (2) can be obtained by the Karhunen–Loève procedure [14, 21, 32–37]. Given an N-dimensional dynamical system,

$$\frac{\mathrm{d}a_j}{\mathrm{d}t} = F_j(a_k) \qquad j, k = 1, 2, \ldots N \tag{13}$$

this technique involves calculating the (Hermitian) correlation matrix $\langle a_j a_k^* \rangle$, where $\langle \cdot \rangle$ denotes an ensemble average, and finding its (orthogonal) eigenvectors and (real) eigenvalues. The eigenvalues give a measure of how much energy, on average, is in each eigenmode. This procedure was carried out for various q when $\rho = c_0 = 0.01$, using time averages taken over several thousand time units. To simplify the computations while still retaining an accurate description of the system, the number of Fourier modes used in the correlation matrix ($\bar{N}$) was chosen to be proportional to $1/q$, based on the Fourier dimension estimates discussed above. (It should be noted that the 'method of snapshots' [36, 37], not used here, allows the use of data vectors of arbitrary length.)

With the measures used for the Fourier dimension in mind, we look at the number of KL eigenmodes required to capture a certain percentage of the ($\bar{N}$-mode) energy of the system and the number required to get a specified drop-off in the eigenvalue spectrum. The results for the q-dependence of d_{KL} when $\rho = c_0 = 0.01$ are shown in table 2. Like d_{F}, d_{KL} was

Table 2. Estimates of the Karhunen-Loève dimension, d_{KL}, using the 10^{-5} drop-off and 99.99% energy capture criteria for the case $\rho = c_0 = 0.01$.

q	$\bar{N}$	10^{-5} drop-off			99.99% energy capture		
		d_{KL}	qd_{KL}	$q^2 d_{\mathrm{KL}}$	d_{KL}	qd_{KL}	$q^2 d_{\mathrm{KL}}$
0.1	63	38	3.8	0.3800	28	2.8	0.2800
0.05	79	76	3.8	0.1900	56	2.8	0.1400
0.025	159	153	3.825	0.0956	114	2.85	0.0713
0.015	267	228	3.42	0.0513	177	2.655	0.0398

found to increase linearly with $1/q$, further evidence that $d_{i,m.} \sim 1/q$ near the dissipationless limit in 1-D. We note that, when $q = 0.05$, the number of KL eigenmodes needed to capture 99.99% of the energy for $\rho = c_0 = 0.01$ (56) was only nine percent greater than the number needed for $\rho = c_0 = 0.25$ (51). This is essentially the same behaviour found for d_{F}.

4.2. Lyapunov dimension calculations

We are interested in the behaviour near the dissipationless limit of the attractor dimension, d_{att}. To study this, Lyapunov exponents were calculated and attractor dimension estimates were obtained using the Kaplan–York formula [38]. This gives the approximate value for the attractor dimension

$$d_{\mathrm{att}} \simeq d_\lambda = M - \frac{\sum_{j=1}^{M} \lambda_j}{\lambda_{M+1}} \tag{14}$$

where M is the smallest integer such that the sum of the largest $M+1$ Lyapunov exponents, $\sum_{j=1}^{M+1} \lambda_j$, is negative. The number d_λ is known as the Lyapunov dimension.

For (2), the M largest Lyapunov exponents were calculated by numerically following $M + 1$ nearby initial conditions and measuring the change in the enclosed M-dimensional volume in Fourier phase space. This same technique has been used by Keefe to study both the CGL equation [18, 22] and plane Poiseuille flow [39]. We calculated the Lyapunov exponents by the standard procedure [40–42] of applying Gram–Schmidt reorthonormalization to the displacement vectors at suitably separated times and averaging over a large number ($\sim 10^3$) of correlation times in order to capture the overall behaviour. Since the non-variational approach was used, the time between samples (i.e. renormalizations) was chosen to give only a small change in the fastest growing displacement vector, so that the local features of the attractor would be captured. For all calculations, the nth initial displacement from the reference trajectory took the form of an $O(10^{-6})$ increase in the amplitude of the nth sine mode.

As noted previously, for Dirichlet, Neumann, and periodic boundary conditions it has been demonstrated for $\rho = c_0 = 0.25$ that $d_{att} \sim 1/q$ when q is sufficiently small [10, 22]. It was predicted in [1] that this generally expected behaviour [43, 44] should continue near the dissipationless limit. Confirmation of this can be seen in our Lyapunov dimension results for $\rho = c_0 = 0.01$, shown in table 3.

Table 3. Results of Lyapunov exponent calculations for the case $\rho = c_0 = 0.01$. Shown for each q are the largest exponent λ_1, the Lyapunov dimension $d_\lambda \simeq d_{att}$ and its product with q, and the number of positive exponents N_+.

q	λ_1	d_λ	qd_λ	$1/q$	N_+
0.1	0.0241	18.05	1.805	10	8
0.05	0.0262	36.98	1.849	20	18
0.025	0.0315	77.89	1.947	40	39

Although only three data points were obtained, the factor of four between the smallest and largest values of q examined indicates that there is very little deviation from the expected linear behaviour. In addition, as found for the case $\rho = c_0 = 0.25$ by Sirovich *et al*, an extrapolation of our attractor dimension estimates to relatively small $1/q$ gives $q \simeq 1$ when $d_{att} = 0$, in agreement with the occurrence of the bifurcation from homogeneous equilibrium at $q = 1$ when $\rho = c_0$.

To examine the effect of ρ and c_0 on d_{att}, Lyapunov exponents and attractor dimension estimates were calculated for several values of $\rho = c_0$ when $q = 0.05$. These results are given in table 4. It can be seen that d_{att} increases as $\rho = c_0$ is decreased. However,

Table 4. Results of Lyapunov exponent calculations for $q = 0.05$ and $\rho = c_0$. Shown are the largest exponent λ_1, the Lyapunov dimension $d_\lambda \simeq d_{att}$ and its product with $c_0^{1/2}$, and the number of positive exponents N_+.

c_0	λ_1	d_λ	$\sqrt{c_0} \cdot d_\lambda$	N_+
0.6	0.1494	22.19	17.19	12
0.25	0.0972	25.33	12.67	15
0.01	0.0263	36.98	3.698	18

while $\rho = c_0$ decreases by a factor of 60, d_{att} only increases by approximately 67%. Thus changing $\rho = c_0$ has a moderate effect on the attractor dimension, although, as seen above, it does not affect the form of the q-bound on d_{att}.

In [1], it is stated that for all μ and ν the bound on the attractor dimension for the 1-D CGL equation is proportional to $R^{1/2}$. The numerical results in [10] for $\rho = c_0 = 0.25$ and those presented here for $\rho = c_0 = 0.01$ (which is taken to represent the dissipationless limit) have confirmed this for $-\mu = \nu$, since in this case $R^{1/2} = q^{-1}$. From the relations connecting the parameters in (2) and (9), it can be seen that in general $R^{1/2} = 2\pi k_L$. Thus, the physical interpretation of the $R^{1/2}$ bound on the attractor dimension is that the number of energy-bearing (i.e., integral-range Fourier) modes determines the dimension of the attractor.

The inertial manifold predictions given in [1] imply that the number of basis functions needed to fully describe the problem is bounded in proportion to a higher power of k_L than is the attractor dimension. This would mean that the attractor is very complicated even when it has a fairly low Lyapunov dimension, an idea which disagrees with our numerical results. For $\rho = c_0 = 0.01$, we found that the number of Fourier modes and the number of KL eigenmodes needed to maintain a fixed degree of accuracy were both directly proportional to $1/q$, the same behaviour found for the attractor dimension.

4.3. A Lyapunov functional

One of the key quantities in the analysis of Bartuccelli *et al* is the set

$$F_n = \int \left[\left| \left(\frac{\partial}{\partial x} \right)^{n-1} A \right|^2 + |A|^{2n} \right] dx \qquad n = 1, 2, \ldots \tag{15}$$

These F_n's are important because they are the Lyapunov functionals for the 1-D NLS equation (8). Bartuccelli *et al* obtain different time-asymptotic R-bounds on F_n for the cases $\rho, c_0 \sim 1$ and $\rho, c_0 \ll 1$. Here we will compare their predictions for

$$F_2 = \int_0^\pi \left[\left| \frac{\partial A}{\partial x} \right|^2 + |A|^4 \right] dx \tag{16}$$

with numerical results for $\rho = c_0 = 0.01$. The bounds in [1] imply that

$$\limsup_{t \to \infty} F_2 \leqslant cq^{-2} \qquad \rho = c_0 \sim 1 \tag{17}$$

$$\limsup_{t \to \infty} F_2 \leqslant cq^{-4} \qquad \rho = c_0 \ll 1. \tag{18}$$

For $\rho = c_0 = 0.01$ and four values of q, the maximum of F_2 obtained from a long time series, denoted F_2^{max}, was taken as the experimental value for $\limsup_{t \to \infty} F_2$. Table 5 contains the results of these calculations. It can be seen that as q decreases F_2^{max} increases

Table 5. Numerical results for the Lyapunov functional F_2 for $\rho = c_0 = 0.01$.

q	F_2^{max}	$q^{3/2} F_2^{max}$	$q^{7/4} F_2^{max}$	$q^2 F_2^{max}$
0.1	6.19	0.196	0.110	0.062
0.05	19.5	0.218	0.103	0.049
0.025	68.7	0.272	0.108	0.043
0.015	173	0.318	0.111	0.039

less slowly than q^{-2} and slightly faster than $q^{-3/2}$. The quantity F_2^{max} was found to be approximately proportional to $q^{-7/4}$. This result for $\rho = c_0 = 0.01$ implies that near the dissipationless limit the asymptotic bounds on F_2 given by Bartuccelli *et al* are too large.

The fact that for $\rho = c_0 \ll 1$ F_2 was found to increase less slowly than q^{-2} suggests that the bounds they give on F_2 for relatively large dissipation are also high. Finally, this overestimate for F_2 near the dissipationless limit suggests an overestimate of the asymptotic bounds on all the F_n's near the 1-D dissipationless limit, and hence a possible overestimate of the bounds on other related quantities (such as $d_{\mathrm{i.m.}}$ and $||A||_\infty^2$). Our results for F_2 support the above numerical results which suggested the calculations in [1] overestimated $d_{\mathrm{i.m.}}$.

Remark. For $\rho, c_0 \ll 1$, Bartuccelli *et al* give an asymptotic bound which implies $\limsup_{t\to\infty} ||A||_\infty^2 \leqslant c \frac{\rho}{q^2 c_0}$. Although we did not make systematic measurements of $||A||_\infty$, our results indicated that it depends only weakly on q (for $\rho = c_0 = 0.01$) and $\rho = c_0$ (for $q = 0.05$), and that it never exceeds the approximate value 1.8.

5. Universal behaviour for $\rho = c_0 \ll 1$

We now discuss some aspects of universality which have been observed in solutions of (2) for $q \leqslant 0.1$. As stated previously, for $\rho = c_0 = 0.25$ the averaged wavenumber spectrum of (2) takes a universal form as a function of qk. Our results for $\rho = c_0 = 0.01$ showed that $d_F \sim q^{-1}$, suggesting universal behaviour in this case also. This universality is confirmed by the plots in figure 15 of $\log[\langle|f_k|^2\rangle/q]$ versus qk.

A more direct form of universality which was found to hold for (2) is that of the Lyapunov exponent spectrum, denoted $\lambda(n)$. If $\lambda(n)$ is plotted against qn, fixing $\rho = c_0 = 0.01$, then the spectra for various q all lie on nearly the same curve. This is done in figure 16. It can be seen that for larger qn this universality holds very accurately. The results for smaller qn would likely be better if longer averages had been used in computing the Lyapunov exponents. For $\rho = c_0 = 0.25$, Keefe [22] found this same universality for both Neumann and periodic boundary conditions.

We note that, in contrast to the wavenumber spectrum, universality in the Lyapunov exponent spectrum requires a rescaling of the index n only. This type of universality is also seen in the one-dimensional Kuramoto–Sivashinsky equation [45]. In that problem L, the parameter analogous to $1/q$, occurs in the boundary conditions instead of in the equation itself, and determines the length of the domain in which the solution evolves. Self-similarity leads to a universal form for the Lyapunov exponent spectrum as a function of n/L. In (2) length can be rescaled via $x' = x/q$ in order to eliminate q from the equation and change the domain to $x' \in [0, \pi/q]$. Therefore, the 1-D CGL problem can be viewed as one in which q determines the length of the one-dimensional 'box' in which the solution evolves. This explains the observed universality in the Lyapunov spectrum and, along with nearly constant total energy, also explains the universality in the wavenumber spectrum.

We now present results indicating the way the Lyapunov exponent spectrum changes near the dissipationless limit. Figure 17 shows the spectra for $\rho = c_0 = 0.25$ and $\rho = c_0 = 0.01$ when $q = 0.05$. It can be seen that the spectrum gets much flatter as the dissipationless limit is approached. This is thought to be related to the fact that both the growth ($\propto \rho A$) and the dissipation ($\propto q^2 c_0 A_{xx}$) are very small for $\rho = c_0 \ll 1$.

6. Remarks on observed wavenumber spectra

The wavenumber scale $k_L = q^{-1}\sqrt{\rho/c_0}$ qualitatively explains the change in the size of the integral range as c_0 (and possibly ρ) becomes small. For these wavenumbers ($k \leqslant k_L$) the
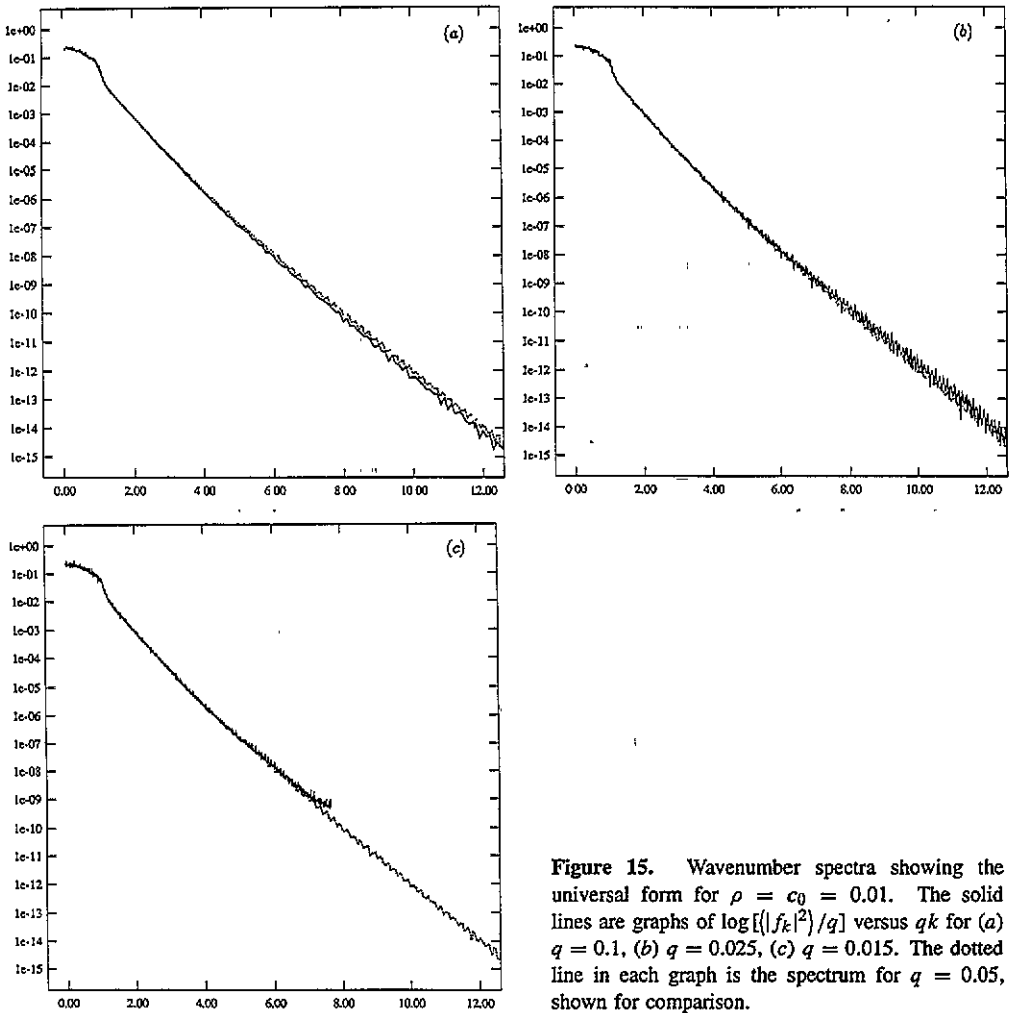
Figure 15. Wavenumber spectra showing the universal form for $\rho = c_0 = 0.01$. The solid lines are graphs of $\log[\langle |f_k|^2\rangle/q]$ versus qk for (a) $q = 0.1$, (b) $q = 0.025$, (c) $q = 0.015$. The dotted line in each graph is the spectrum for $q = 0.05$, shown for comparison.

mean square amplitude $\langle |f_k|^2\rangle$ is approximately constant, while for very high wavenumbers $(k \gg k_L)$ it decays exponentially.

Of interest here is the prediction in [10] that for wavenumbers outside the integral range

$$\langle |f_k|^2\rangle \sim (qk)^{-4}e^{-qk}. \tag{19}$$

For $qk \sim 1$ this result describes the transitional region between the constant amplitude modes and those which decay exponentially with increasing k. In [10] the result (19) was confirmed for $\rho = c_0 = 0.25$ via numerical simulations. Since ρ and c_0 were fixed, the derivation of (19) was done without particular consideration for the dependence on these parameters.

Here we note that outside the integral range the wavenumber spectra observed in the present study for $\rho = 0.25$, $c_0 \ll 1$ are well described by a function of the form

$$F(k) \sim q^{-4}(k + k_0)^{-4}e^{-\alpha q k} \tag{20}$$

it being assumed that $k + k_0 > 0$. Generally $\alpha \sim 1$, but k_0 was found to depend on c_0 and is thought to be related to k_L. It remains to establish the exact parameter dependence of k_0
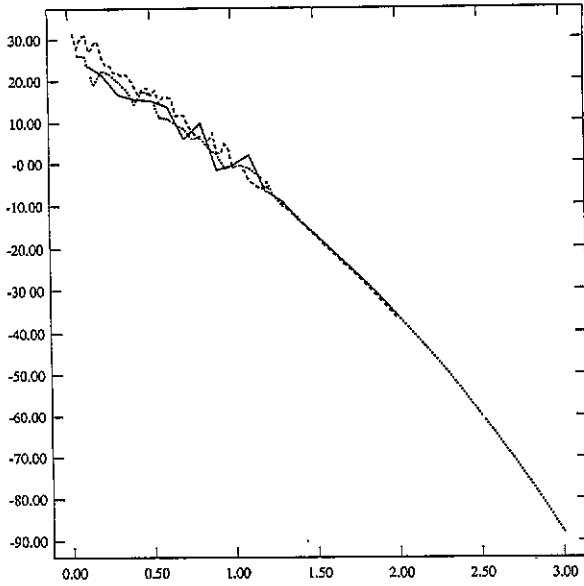
Figure 16. Lyapunov exponent spectra showing the universal form for $\rho = c_0 = 0.01$. We plot $\lambda(n)$ versus qn for $q = 0.1$ (—), 0.05 ($\cdots$) and 0.025 (- - -).
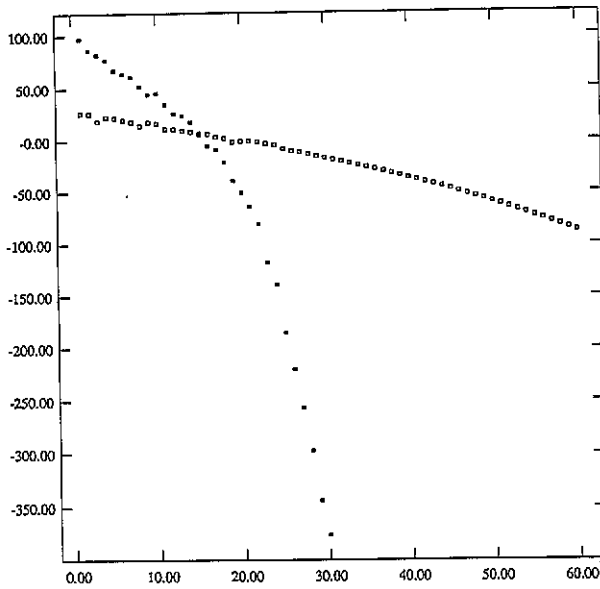

Figure 17. Lyapunov exponent spectra when $q = 0.05$ for $\rho = c_0 = 0.25$ (■) and $\rho = c_0 = 0.01$ (□). Here we plot $\lambda(n)$ versus n.

and to fully understand the transitional region between the integral and dissipative ranges for $\rho = c_0 \ll 1$.

7. Conclusion

Our numerical results in sections 2 and 3 showed that hard turbulence does not occur in solutions of the 1-D CGL equation subject to Dirichlet boundary conditions when the

dissipation becomes very small. This confirmed the general predictions made in [1]. Our results in section 4 for $\rho = c_0 \ll 1$ showed that the attractor dimension continues to scale like $1/q$, as expected, and that the inertial manifold for this case is much simpler than was suggested in [1]. Finally, in section 5 we showed for $\rho = c_0 \ll 1$ that the universality found in [10] for the wavenumber spectrum continues to hold, and that the Lyapunov spectrum also has a universal form when the index is scaled by $1/q$.

The occurrence of small length scales in the 1-D CGL equation was found to be limited more by their production than by their dissipation. This is clear from the fact that the wavenumber spectrum changed very little as the dissipationless limit was approached, even when δ_d was decreased by a factor of ten. The absence of the large localized fluctuations generally associated with hard turbulence could explain both the non-production of small length scales and the absence of an inertial range. It is felt that for an inertial range to occur in the CGL equation it is necessary to have not only a significant separation between integral and dissipative length scales, but also some mechanism for producing an intense cascade of energy to high wavenumber modes. As discussed in [1], both of these conditions are expected to hold near the dissipationless limit in 2-D due to the existence of solutions to the 2-D NLS equation which become infinite in finite time.

Acknowledgments

References

[1]   Bartuccelli M, Constantin P, Doering C R, Gibbon J D and Gisselfalt M 1990 On the possibility of soft and hard turbulence in the complex Ginzburg–Landau equation *Physica* **44D** 421–44
[2]   Stewartson K and Stuart J T 1971 Non-linear instability in plane Poiseuille flow *J. Fluid Mech.* **48** 529–45
[3]   Kogelman S and DiPrima R C 1970 Stability of spatially periodic supercritical flows in hydrodynamics *Phys. Fluids* **13** 1–11
[4]   Kuramoto Y 1978 Diffusion induced chaos in reaction systems *Progr. Theor. Phys. Suppl.* **64** 346–67
[5]   Kuramoto Y and Koga S 1982 Anomalous period-doubling bifurcations leading to chemical turbulence *Phys. Lett.* **92A** 1–4
[6]   Kuramoto Y and Yamada T 1976 Turbulent state in chemical reactions *Progr. Theor. Phys.* **56** 679–81
[7]   Hocking L M, Stewartson K and Stuart J T 1972 A nonlinear instability burst in plane parallel flow *J. Fluid Mech.* **51** 705–35
[8]   Benney D J and Roskes G J 1969 Wave instabilities *Stud. Appl. Math.* **48** 377–85
[9]   Newell A C and Whitehead J A 1969 Finite amplitude, finite bandwidth convection *J. Fluid Mech.* **38** 279–303
[10] Sirovich L, Rodriguez J D and Knight B 1990 Two boundary value problems for the Ginzburg–Landau equation *Physica* **43D** 63–76
[11] Shraiman B I, Pumir A, van Saarloos W, Hohenberg P C, Chate H and Holen M 1992 Spatiotemporal chaos in the one-dimensional complex Ginzburg–Landau equation *Physica* **57D** 241–48
[12] Cross M C and Hohenberg P C 1993 Pattern formation outside of equilibrium *Rev. Mod. Phys.* **65** 851–1112
[13] Newton P K and Sirovich L 1986 Instabilities of the Ginzburg–Landau equation: periodic solutions *Quart. Appl. Math.* **44** 49–58
[14] Sirovich L and Rodriguez J D 1987 Coherent structures and chaos: a model problem *Phys. Lett.* **120A** 211–14
[15] Newell A C 1974 Envelope Equations *Nonlinear Wave Motion* ed A C Newell (Providence, RI: American Mathematical Society) 157–63
[16] Moon H T, Huerre P and Redekopp L G 1982 Three-frequency motion and chaos in the Ginzburg–Landau equation *Phys. Rev. Lett.* **49** 458–60

[17] Moon H T, Huerre P and Redekopp L G 1983 Transitions to chaos in the Ginzburg–Landau equation *Physica* **7D** 135–50
[18] Keefe L R 1985 Dynamics of perturbed wavetrain solutions to the Ginzburg–Landau equation *Stud. Appl. Math.* **73** 91–153
[19] Deissler R J 1985 Noise-sustained structure, intermittency, and the Ginzburg–Landau equation *J. Stat. Phys.* **40** 371–95
[20] Nozaki K and Bekki N 1983 Pattern selection and spatiotemporal chaos in the Ginzburg–Landau equation *Phys. Rev. Lett.* **51** 2171–74
[21] Rodriguez J D and Sirovich L 1990 Low-dimensional dynamics for the complex Ginzburg–Landau equation *Physica* **43D** 77–86
[22] Keefe L 1989 Properties of Ginzburg–Landau attractors associated with their Lyapunov vectors and spectra *Phys. Lett.* **140A** 317–22
[23] Bazhenov M V, Rabinovich M I and Fabrikant A L 1992 The 'amplitude'-'phase' turbulence transition in a Ginzburg–Landau model as a critical phenomenon *Phys. Lett.* **163A** 87–94
[24] Bartuccelli M, Constantin P, Doering C R, Gibbon J D and Gisselfalt M 1989 Hard turbulence in a finite dimensional dynamical system? *Phys. Lett.* **142A** 349–56
[25] Bartuccelli M, Constantin P, Doering C R, Gibbon J D and Gisselfalt M 1990 *Phys. Lett.* **145A** 476 (erratum)
[26] Luce B P and Doering C R 1993 Scaling of turbulent spike amplitudes in the complex Ginzburg–Landau equation *Phys. Lett.* **178A** 92–8
[27] Heslot F, Castaing B and Libchaber A 1987 Transitions to turbulence in helium gas *Phys. Rev.* A **36** 5870–73
[28] Castaing B, Gunaratne G, Heslot F, Kadanoff L, Libchaber A, Thomae S, X-Z Wu, Zaleski S and Zanetti G 1989 Scaling of hard thermal turbulence in Rayleigh–Bénard convection *J. Fluid Mech.* **204** 1–30
[29] Goldman D and Sirovich L A novel method for simulating the complex Ginzburg–Landau equation *Quart. Appl. Math.* in press
[30] Goldman D, Everson R and Sirovich L The two-dimensional complex Ginzburg–Landau equation in the dissipationless limit, in preparation
[31] Rasmussen J Juul and Rypdal K 1986 Blow-up in nonlinear Schrödinger equations–I a general review *Phys. Scr.* **33** 481–97
[32] Loève M M 1955 *Probability Theory* (New York: Van Nostrand)
[33] Karhunen K 1946 Zur Spektraltheorie stochastischer Prozesse *Ann. Acad. Sci. Fenn.* **1** 34
[34] Lumley J L 1967 *Atmospheric Turbulence and Radio Wave Propagation* (Moscow: Nauka)
[35] Lumley J L 1970 *Stochastic Tools in Turbulence* (New York: Academic)
[36] Sirovich L and Park H 1990 Turbulent thermal convection in a finite domain: Part I, Theory *Phys. Fluids* A **2** 1649–58
[37] Sirovich L and Kirby M 1987 Low-dimensional procedure for the characterization of human faces *J. Opt. Soc. Am.* **4** 519–24
[38] Kaplan J and Yorke J 1979 Chaotic behaviour of multidimensional difference equations *Functional differential equations and approximation of fixed points* ed H O Peitgen and H O Walter (Berlin: Springer) p 228
[39] Keefe L, Moin P and Kim J 1987 Is Navier–Stokes turbulence chaotic? *Bull. Am. Phys. Soc. Ser. II* **32** 2026
[40] Shimada I and Nagashima T 1979 A numerical approach to ergodic problem of dissipative dynamical systems *Prog. Theor. Phys.* **61** 1605–16
[41] Benettin G, Galgani L, Giorgilli A and Strelcyn J-M 1980 Lyapunov characteristic exponents for smooth dynamical systems and for Hamiltonian systems: a method for computing all of them *Meccanica* **15** 9–30
[42] Wolf A, Swift J B, Swinney H L and Vastano J A 1985 Determining Lyapunov exponents from a time series *Physica* **16D** 285–317
[43] Ghidaglia J M and Heron B 1987 Dimension of the attractors associated to the Ginzburg–Landau partial differential equation *Physica* **28D** 282–304
[44] Doering C, Gibbon J D, Holm D and Nicolaenko B 1987 Exact Lyapunov dimension of the universal attractor for the complex Ginzburg–Landau equation *Phys. Rev. Lett.* **59** 2911–14
[45] Manneville P 1985 Liapounov exponents for the Kuramoto-Sivashinsky model *Macroscopic Modelling of Turbulent Flows* ed U Frisch, J B Keller, G Papanicolaou and O Pironneau (Berlin: Springer) 319–26